# Posture-invariant three dimensional human hand statistical shape model

Yang, Y.; Yuan, T.; Huysmans, T.; Elkhuizen, W.S.; Tajdari, F.; Song, Y.

**DOI**
10.1115/1.4049445

**Publication date**
2020

**Document Version**
Accepted author manuscript

**Published in**
Journal of Computing and Information Science in Engineering

# Posture-invariant 3D Human Hand Statistical Shape Model

**Yusheng Yang**
School of Mechatronic Engineering and Automation, Shanghai University, China
Faculty of Industrial Design Engineering, Delft University of Technology, The Netherlands
y.yang-9@tudelft.nl

**Tianyun Yuan**
Faculty of Industrial Design Engineering, Delft University of Technology, The Netherlands
T.Yuan@tudelft.nl

**Toon Huysmans**
Faculty of Industrial Design Engineering, Delft University of Technology, The Netherlands
T.Huysmans@tudelft.nl

**Willemijn S. Elkhuizen**
Faculty of Industrial Design Engineering, Delft University of Technology, The Netherlands
w.s.elkhuizen@tudelft.nl

**Farzam Tajdari**
Faculty of Industrial Design Engineering, Delft University of Technology, The Netherlands
F.Tajdari@tudelft.nl

**Yu Song**[1]
Faculty of Industrial Design Engineering, Delft University of Technology, The Netherlands
y.song@tudelft.nl

**ABSTRACT**
*A high-fidelity digital representation of (part of) the human body is a key enabler for integrating humans in a digital twin. Among different parts of human body, building the model of the hand can be a challenging task due to the posture deviations among collected scans. In this paper, we proposed a posture invariant statistical shape model (SSM) of the human hand based on 59 3D scans of human hands. First, the 3D scans were spatially aligned using a Möbius sphere-based algorithm. An articulated skeleton, which contains 20 bone segments and 16 joints, was embedded for each 3D scan. Then all scans were aligned to*

[1] Corresponding author: y.song@tudelft.nl

*the same posture using the skeleton and the linear blend skinning (LBS) algorithm. Three methods, i.e. Principal Component Analysis (PCA), kernel-PCA (KPCA) with different kernel functions, and Independent Component Analysis (ICA), were evaluated in the construction of the SSMs regarding the compactness, the generalization ability and the specificity. The PCA-based SSM was selected, where 20 principal components were used as parameters for the model. Results of the leave-one-out validation indicate that the proposed model was able to fit a given 3D scan of the human hand at an accuracy of 1.21 ± 0.14 mm. Experiment results also indicated that the proposed SSM outperforms the SSM that was built on the scans without posture correction. It is concluded that the proposed posture correction approach can effectively improve the accuracy of the hand SSM, therefore enables its wide usage in human integrated digital twin applications.*

## 1. INTRODUCTION

In the past decade, the Digital Twin [1] attracted wide interests for its ability to reduce costs and risks, improving the efficiency in product design and manufacturing, etc. [2]. Recently, the human integration in the digital twin has received increased attention in many applications [3], e.g. for empowering operators [4], monitoring and managing athletes' fitness activity and results [5], personalized product design [6]. In different applications of human integrated digital twin, a parameter-driven high-fidelity model of (part of) the human is one of the key enablers, as it can be quickly adjusted/updated to fit the geometric shape of individuals for different needs [7][8]. For instance, Yu et al. [9] proposed an approach for the design of gloves controlled by parameters of a digital hand model. By categorizing the foot shape into several clusters and based on the statistical analysis of each cluster, Baek and Lee [10] proposed a method for mass-customization of footwear. Harih and Dolsak found that a tool-handle design based on

the hand SSM had 25% larger contact areas than using traditional cylindrical hand models [11]. The enlarged contact areas contributed to a better grip as well as reduced possibilities of being affected by cumulative trauma disorders.

A statistical shape model (SSM) of the human hand, which can represent the 3D hand shape with a limited number of parameters with a certain accuracy, can be utilized as a high-fidelity digital representation of the hand in many applications [12]. However, the human hand has complicated structures. Consisting of 27 bones, each hand has 27 degrees-of-freedom (DOF), of which 14 are located in the fingers [13]. While it is a marvel of dexterity, the complicated structure also posts challenges on both data acquisition and model construction.

Due to aspects like the large number of DOFs, anatomical variations, as well as the difficulty in accurately communicating a posture, it is difficult or even impossible to instruct subjects to take the exact same posture. Differences among postures in the acquired data will lead to large errors in the construction of an SSM. For instance, the posture variation was noticeable in the SSM [14] which was built on the original scans without posture adaptations. Furthermore, the hand is not always steady, and the steadiness depends on for instance the age [15] and the gender [16] of the subject. High speed 3D scanners are generally needed for digitizing the hand shape.

This paper proposes an accurate hand SSM, built from 3D scans with posture corrections. The main contributions of this paper are: 1) A 3D dataset of human hands was collected for building the SSM; 2) A hand skeleton generation method was proposed to align the 3D scans to a “standard posture”; 3) An mean model calculation

algorithm was developed for finding the optimal mean model for the SSM and 4) Different dimensionality reduction methods for generating the hand SSM were evaluated and the principal component analysis method was selected to build the hand SSM. The generalization error of the proposed SSM is 1.21 ± 0.14mm.

The remainder of this paper is arranged as follows: In Section 2, a brief overview of the related work is given regarding human hand SSMs, their construction methods, and the accuracy. The proposed posture correction approach is illustrated in Section 3, and several hand SSMs based on PCA, kernel PCA (KPCA) [17] and independent component analysis (ICA) [18] [19] were built with the aligned models, respectively. In Section 4 we compared the properties of these models and the PCA-based SSM was selected. This model was further validated and compared against the hand SSM without posture correction in Section 5. Finally, a short conclusion is drawn where the future works are highlighted as well.

## 2. RELATED WORK

### 2.1 Human body statistical shape model

The SSMs of (different parts of) human body have been extensively studied in the past decades [20]. In the construction of an SSM, the 3D shape variations of the captured human body shapes are affected by the postures globally and locally, which are both needed to build the statistical model(s). In the past researchers tried to acquire data with “standard postures”, e.g. by use of foot placement guides and verbal instructions in the CAESAR project [21], however it was found that the inter-subject differences made it difficult for participants to position their joints in the same angles.

A common approach to correct these deviations is to introduce an articulated skeleton to the 3D model [22][23], and utilizing freeform deformation algorithms, e.g. linear blend skinning (LBS) or as-rigid-as-possible (ARAP) approaches [24], to deform the 3D body shapes towards a standard posture. Examples of those studies include the work of Hasler et al.[25], where the pose of the human was governed by an embedded skeleton. Another skeleton-based human model is the Skinned Multi-Person Linear (SMPL) model [26], where the pose-dependent 3D shapes are a linear function of the elements of the pose rotation matrices. Besides the skeleton based methods, Wuhrer et al. [27] proposed a posture invariant statistical shape analysis method based on a local representation that is obtained by using the Laplace operator. However, it is computationally expensive since it needed to solve an optimization problem for each vertex. Danckaers et al. [28] [14] proposed a framework for building a posture invariant SSM which includes SSM construction, feature modification, identity removal, and posture normalization these four steps. The advantage of this framework is that many parameters, such as gender, age, and arm length, can also be embedded for a more accurate approximation.

In the modelling of 3D human hands, articulated skeletons were also introduced in many computer vision and computer-aided design (CAD) applications. For instance, for tracking the joints of human hands, Oikonomidis et al. [29] utilized a hand model which consisted of 62 3D geometric primitives with 26 DOFs. Though it was easy to use, it cannot describe the details of a hand due to the simplified geometry. Another articulated hand model was developed by Sridhar et al. [30] [31]. It consisted of 32

joints with 26 DOFs and was used for hand tracking based on RGB-D images. Tkach and Tagliasacchi [32] also proposed one sphere-mesh based hand template to fit the geometry of the hand by adjusting the positions and radii of the skeleton vertexs. The MANO hand model proposed by Romero et al. [33] is a hand SSM based on the data collected from 31 subjects. It utilizes 15 joints and is able to approach a hand using a combination of shape and pose parameters. Table 1 summarizes those hand models in the literature regarding its geometry, DOFs, accuracy, etc.

Currently, research on the development of the hand SSM mainly focuses on the accuracy, the validity, the flexibility and the efficiency of the models [34]. However, not all models are suitable for digital twin applications, e.g. the meshes of the some SSMs [29] are not dense enough to represent the surface undulation, the specificity of the hand model was not extensively discussed, the data-driven hand model [33] may fail when a posture falls outside the pose space. Besides, the fitting speed of using the model to approach a specific subject should be fast enough for a quick response in the digital twin applications.

**2.2 Model Registration**

Finding the correspondence between different 3D hand shapes is an important step in the process of building an SSM [35]. In the past, many algorithms were developed to tackle this problem. For instance, Amberg et al. [36] presented a non-rigid iterative closest point (ICP) approach for registering two shapes by iteratively minimizing a cost function which consists of the distance term, the stiffness term, and the landmark term. By involving a Markov Random Field (MRF) optimization into the isometric

embedding process, Chen and Koltun [37] proposed a simple non-rigid registration algorithm for 3D surfaces. Ma et al. [38] introduced the non-rigid point set registration method by taking the advantages of Gaussian mixture models, which was able to robustly preserve both global and local structures during matching. The dense point-to-point correspondence algorithm proposed by Lee and Kazhdan [39] is a novel non-rigid registration algorithm for watertight objects. By mapping objects to unit Möbius spheres using a conformal map, the alignment between meshes can be established by performing Fast Fourier Transformation (FFT), and the registration is refined based on the optical flow.

**2.3 Dimension Reduction**

For building an effective as well as compact SSM, dimensionality reduction techniques are often applied to capture the principle information of the shape variations with the least possible parameters. The PCA method is one of the most popular approach in statistical modeling [40]–[42]. For instance, Pishchulin et al. [43] built a SSM of human body based on the 3D scans using the PCA. Similar works can be found in Allen et al. [44] where the SSM was built on 250 human body scans. The KPCA method is a nonlinear extension of the PCA by mapping the input data to a higher dimensional space with different types of kernel functions. An example application of using KPCA in the construction of the SSM is the active shape model segmentation developed by Kirschner et al. [45]. Independent Component Analysis (ICA) is another dimensionality reduction method which utilizes the independent non-Gaussian components from the mixture variables [18], and it is widely used for solving blind

source separation problems [19]. In a comparison of using the PCA, the KPCA and the ICA methods in constructing an SSM of the left ventricle, Roohi and Zoroofi [46] found that using the KPCA method was more appropriate regarding the accuracy of the SSM. However, which method is most suitable for constructing an SSM specifically for the hand remains unknown.

## 3. APPROACH

In order to build a posture invariant hand SSM, the following steps are undertaken (also see Fig. 1). First, 3D scans of the human hands were collected using two different 3D scanners. After post-processing, one scan was selected as a template and a predefined articulated skeleton was embedded therein. All acquired data was then registered to the template and the predefined skeleton was mapped to all aligned scans. Using the embedded skeleton, all the scans were deformed to a same posture, and the SSM was built on those scans. The rest of this section presents the details of each step.

### 3.1 Data Acquisition

Data collection was conducted at multiple sites using two different 3D scanners. Part of the data was captured by a hand scanning system which consisted of five 3DMD modular units. For short range scanning, which we are using, the system has a mean global accuracy of 0.2 mm [47]. Other scans were captured by a hand scanner developed in our previous work [48]. This scanner utilizes 50 camera modules and close-range photogrammetry technique, and is able to achieve a mean absolute error (MAE) of 0.38 mm.

Before data collection, informed consents were acquired from subjects. During the scanning process, all subjects were asked to position their right hand with a "standard posture", i.e. keeping the palm flat and all fingers extended and abducted. The purpose of this step was to provide a good initial posture for posture alignment in the following steps. In total we collected 59 3D scans of human hands, where 32 were acquired by the 3DMD system and 27 were acquired by the self-developed hand scanner. Among those scans, 12 were collected from female subjects and 47 were males.

Since the original scans may have some holes and spikes, during the post-processing, holes in the scans were filled [49], and spikes were removed. Next, triangles representing the forearm, i.e. up to the distal sides of the radius and the ulna, were removed. One scan was selected, further refined and used as a template to wrap all other scans utilizing the program Wrap 3.4 [50]. Thus, all scans after post-processing can be described by the same number of vertices and triangles. Given a scan, it can be represented as $M\left((V,F)\middle|V=\left(v_1,v_2,\cdots,v_j,\cdots,v_{N_v}\right),F=\left(f_1,f_2,\cdots,f_k,\cdots,f_{N_f}\right)\right)$, where $V$ is a set of vertices in the mesh and $F$ is a set of faces. $v_j$ is the 3D Cartesian coordinate of the $j_{th}$ vertex in $V$, $N_v$ is the number of vertices, $f_k$ is the $k_{th}$ triangle in $F$, and $N_f$ is the number of triangles (in this paper, $N_v = 33270$, $N_f = 66536$). The dataset $D_M$ of all processed scans is $D_M = \{M_1, M_2, \cdots, M_N\}$, where $N$ denotes the number of scans and in this paper, $N = 59$. Fig. 2 presents some examples of scans before and after post-processing.

**3.2 Registration**

In the post processing process, all hand scans in $D_M$ were wrapped by a template $M_T$, therefore each scan $M_i$ had the same number of vertices and faces. However, the vertices in $M_i$ did not have vertex-to-vertex correspondences to $M_T$, thus a registration process was needed to find the corresponding vertices among hand models. Establishing the correspondence between scans in $D_M$ and the template is a key step in building an SSM. There are many ways to establish the correspondence between two meshes, e.g. using non-rigid ICP registration algorithms. In this paper, we adopted the algorithm developed by Lee and Kazhdan [39] to register the template $M_T$ to each mesh $M_i$ in $D_M$ for establishing a map as $M_i|M_T \rightarrow M_i$. The algorithm converts the correspondence problem between two meshes into the registration problem over two depicted spheres using the following steps: 1) Computing the conformal parameterization of the mesh over the sphere. In this step, the conformalized mean curvature flow is utilized to parameterize the genus-zero surface over the unit sphere [51]. With the mean curvature flow, the vertex on the surface is pushed towards the average position of its neighbors, i.e. the mesh surface evolves towards a smoother shape. Eventually, the surface after utilizing the conformalized mean curvature flow is converged onto the sphere; 2) Authalic evolution. As the conformal parameterization of the mesh over a sphere may lead to the extreme compressive areas on the sphere, an authalic evolution approach is adopted [39] to decompress those areas; 3) Compute the Heat Kernel Signature (HKS) [52] of each vertex in the source and the target meshes, where the scan $M_i$ and the template $M_T$ can be represented as $K_{M_i}$ and $K_{M_T}$, respectively; 4) Rotational alignment.

In this step, the correspondence between two mesh is established by finding the rotational $R^*$ that maximizes the correlation between $K_{M_i}$ and $K_{M_T}$ as [39]:

$$R^* = arg \max_{R \in SO(3)} \langle R(K_{M_i}), K_{M_T} \rangle_{S^2} \quad (1)$$

where the inner-product $\langle \cdot \rangle_{S^2}$ is obtained by integrating the point-wise product of the HKS of vertices over the sphere [39]. $R(K_{M_i})$ describes the rotation result of $K_{M_i}$ by the rotation $R$. Furthermore, a registration refinement process is conducted by using the optical flow to improve the accuracy of the correspondence performance.

**3.3 Hand Posture Correction**

After the registration, each hand model $M_i$ in $D_M$ can be represented as a triangular mesh with $N_v$ vertices and $N_f$ triangular faces, and vertices are relatively in the same positions on the hand object, i.e. they have a vertex-to-vertex correspondence. To be able to correct the differences among postures, a posture correction method was developed based on the embedded skeleton and following the principle that if the skeletons of two hands are in the same pose, then the corresponding meshes are also in the same posture. The proposed posture correction method has 3 steps: 1) skeleton generation; 2) skeleton posture correction and 3) skin deformation. In the first step, an articulated skeleton was developed based on previous work [53] [54] and embedded to the template. The skeleton is defined based on 20 bones and 16 joints, including nine hinge joints, six condyloid joints, and a base joint, accounting for 27 DOFs (including 3 global orientations and 3 translations). For specifying the joint location in the template, we manually segmented the surface of the template model into $N_K = 16$ parts following its anatomical landmarks and defined the

relationships between the joint locations and the segmented 3D shapes as Fig.4(a). For instance, assuming the interphalangeal joints are located in the center of the finger knuckles, the 3D position of a joint is calculated as the geometric mean of the corresponding finger segment boundaries. The wrist joint is taken as the mean of the vertices in the wrist plane. The palm joint is located at the geometric center of the palm. Besides those joints, five fingertip key points are specified to describe the distal phalanges. As the vertex-to-vertex correspondence has been established between the template and other scans after registration, for a vertex in the template, the position of its corresponding vertex on the other hand model is located at nearly the same position as this vertex regarding the template hand shape. For instance, for the vertices stand for the knuckle boundary in the template model, their corresponding vertices on the other scans can be used to describe the knuckle boundary of that hand as well. When the vertices that determine the positions of joints are known on the template, the corresponding vertices on the other scans can be identified, and the positions of joints can be calculated accordingly. Using this method, the skeleton for each hand scan can be established based on the template.

In the skeleton, bones and joints are organized hierarchically with the parent-child relationship as illustrated in Fig. 4(b). Each bone is represented by a segment between joints and it is denoted as $B(J_{parent}, J_{child})$, and $J_1$ is the root joint. For fingertip bones, $J_{child}$ is the position of the corresponding fingertip key point. Using this representation, the skeleton $L$ of the hand model can be described with $L\left(B_1(J_{parent_1}, J_{child_1}), \cdots, B_{N_b}\left(J_{parent_{N_b}}, J_{child_{N_b}}\right)\right)$, where $N_b$ is the number of bones.

Embedding this skeleton in the hand model, a hand model $M_i$ that contains both the surface mesh and the skeleton is described as $M(V, F, L)$.

For each bone in the skeleton, a local coordinate system is defined where the origin is set to be the parent joint. Taking the example of two adjacent bones composed of three joints as illustrated in Fig. 4(c). In the figure, the x-axis of the coordinate system for $J_i$ points towards $J_{i+1}$, the y-axis is perpendicular to the plane defined on joints $J_{i-1}$, $J_i$ and $J_{i+1}$, and the z-axis is generated using the right-hand rule. Rotation matrix $Q_B$ indicates the relative rotation of x-axis between the current local coordinate and the articulated coordinate it based on. The homogenous transformation matrix $T_B$ between $B(J_{i-1}, J_i)$ and $B(J_i, J_{i+1})$ can be defined as:

$$T_{B_i} = \begin{bmatrix} Q_{B_i} & l_{B_{i-1}} \\ 0 & 1 \end{bmatrix} \epsilon R^{4\times 4} \tag{2}$$

where $Q_{B_i}$ is the rotation matrix and $l_{B_{i-1}}$ is the length of bone $B(J_{i-1}, J_i)$. Based on the definition of $T_B$, a particular posture of human hand can be represented as $G(M) = \left(T_{B_1}, T_{B_2}, \cdots, T_{B_{N_b}}\right)$, and the transformation matrix from the world coordinate to the local coordinate of bone $B(J_i, J_{i+1})$ is $H_B = T_1 \cdots T_{p_B} T_B$, where $T_{p_B}$ is the parent coordinate system corresponding to $T_B$. All local coordinates systems are presented in Fig. 4(d).

For building a posture invariant SSM, all models in $D_M$ should have the same posture as that of the template $M_T$. In the second step, the skeletons of them were aligned. Given a hand model $M$ and the template model $M_T$, both posture parameters can be extracted as $G(M)$ and $G(M_T)$. Here we define the same posture of hand as they

have the same rotation matrix $Q_{B_k}$, i.e., all fingers have the same orientation. For instance, suppose $B_{i-1}$ and $B_{i-1}^T$ are already aligned, to align $B_i$ to $B_i^T$, the relative rotation matrix of $B_i$ can be calculated by $\mathbb{T}_i = Q_{B_i^T} \cdot Q_{B_i}^{-1}$ as shown in Fig. 5. Then the target position $B_i'$ can be computed by $B_i' = \mathbb{T}_i \cdot B_i$. As only the rotation part in the transformation matrix is updated, the length of the bone is not changed.

In the third step, to deform the mesh together with the skeleton, we introduced the linear blend skinning (LBS) algorithm [55]. Using this algorithm, a new position of a vertex can be computed through a weighted transformation of the associated bones as $v_j' = \sum_{i=1}^{N_b} w_i(v_j)\mathrm{T}_i v_j^i$, where $w_i(v_j)$ is the weight function of the $i_{th}$ bone associated with the vertex $v_j$. The deformation result based on the LBS algorithm can be significantly influenced by the weights, where unsuitable weights may cause discontinuities and show the "candy wrapper" effect when the bone undergoes a twisting motion. To avoid the discontinuities and produce smooth and intuitive deformation of the hand model, the bounded biharmonic weights between the surface vertexes and the bones were computed by solving the optimization problem of the Laplacian energy subject to bound constraints [56]. For each model in $D_M$, the posture correction algorithm was processed with the computed bounded biharmonic weights. And the 3D scan dataset $D_M$ can be updated to a new dataset $D_M^c$ where the postures of scans were aligned. Fig. 6(a) presents the template model and Figure 6(b) and (c) shows two examples of 3D scans before and after posture correction.

**3.4 The Statistical Shape Models**

An SSM represents the mean shape of the population and its variations in shape where the distribution of the shape variation is with respect to the mean model. One thing that needs to be addressed here is that even though the vertexes correspondence and the skeleton alignment were processed among models in $D_M^c$ in the above steps, the spatial orientation of the models was not aligned yet. Therefore, all models in the dataset were aligned to the template model using the rigid ICP algorithm, then the mean model for computing the SSM was generated based on aligned models. Each vertex of the mean model was calculated as $V_m^{mean} = (1/N)\sum_{i=1}^{N}(V_m^i)$ where $m$ is the index of the vertex, $V_m^i$ is its corresponding vertex in the $i_{th}$ model and $N$ is the number of models. However, such mean model can be strongly influenced by the selected template as the size and the shape of the template might influence the outcomes of the rigid registration. The General Procrustes Analysis (GPA) [57] method provides a way for aligning and computing the mean shape, but during the process of superimposing all instances to the reference model, the influence of the size of the hand, which is an important property of the hand, is eliminated. In this research, we proposed Algorithm 1 based on GPA to find the optimal mean model. Using the Algorithm 1, the mean model was iteratively updated in each iteration until an optimal was achieved. Fig. 7 illustrates the RMSE between the updated mean model $M_{new}$ and the current mean model $M_{mean}$ regarding the number of iterations in Algorithm 1.

| **Algorithm 1** | Computing the optimal mean model |
|---|---|
| **Input:** | $D_M$, *Threshold*, $Max_{iteration}$ |
| **Output:** | $M_{mean}$ |
| 1: | *iter* = 0 |
| 2 | $M_{mean}$ = *the mean model of* $D_M$ |
| 3: | *error = INF* |

4: **while** *error* > *Threshold* **do**
5: $D'_M = []$
6: **for** $M_i$ *in* $D_M$ **do**
7: $M'_i$ = $M_i$ *registered to the* $M_{mean}$
8: $D'_M.append(M'_i)$
9: **end for**
10: $M_{new}$ = *the mean model of* $D'_M$
11: *error = RMSE between* $M_{new}$ *and* $M_{mean}$
12: $M_{mean} = M_{new}$
13: $D_M = D'_M$
14: *iter* ++
15: **if** *iter* >= $Max_{iteration}$ **then**
16: **Break**
17: **end while**

Based on the mean model found in Algorithm 1, to investigate the population variance in $D_M^c$, three dimensionality reduction methods, named PCA, KPCA and ICA, were used to construct SSMs of the hand. With those methods, different feature vectors that can describe the shape variance of the hand model were investigated. An SSM can be represented as the mean model plus the combination of those feature vectors:

$$V_{M_{new}} = V_{M_{mean}} + \phi(\gamma_{N_p}) \tag{3}$$

where $V_{M_{mean}}$ denotes the mean model and $V_{M_{new}}$ is the newly generated model. $N_p$ represents the number of feature vectors that used for reconstruction, and $\gamma_{N_p}$ is the corresponding coefficients. Function $\phi(\cdot)$ has different meanings regarding different methods. For PCA, the feature vectors are a number of uncorrelated vectors which are named the principal components (PCs). $\phi(\cdot)$ expresses the linear combination of those PCs, e.g. $\phi(\gamma_N) = \sum_{j=1}^{N_p} \gamma_{N_j} PC_j$. KPCA is the non-linear extension of PCA and the resulted principal components are based on the selected kernel function. Two types of kernel functions were used in this paper to construct the SSM: The Radial Basis Function

(RBF) and the Polynomial function (PF). With the chosen kernel function, the principal components for KPCA can be calculated and $\phi(\cdot)$ expresses the progress of reconstruction based on those components. More details of model reconstruction based on KPCA can be found in [58], [46] and [59]. Different from PCA and KPCA, the feature vectors found based on the ICA method [19] are named independent components (ICs). The reconstruction function $\phi(\cdot)$ of using the ICA can be expressed as a weighted sum of those independent components. There are several methods to find the importance of each IC regarding the SSM [18]. In the proposed research, we projected all data on each IC, then sorted the ICs in descending order, based on the variance of the projected data, where the larger the variance is, the more important this IC is.

## 4. SELECTION OF CONSTRUCTION METHODS

In this section, the performance of the SSM generated based on PCA, RBF-KPCA, PF-KPCA and ICA are evaluated in terms of the compactness, the generalization ability and the specificity [60]. Using the approach proposed in the previous section, we built 5 SSMs based on the posture invariant hand model dataset which consists of 59 scans, each has uniformly distributed 33270 vertices and 66536 faces. These 5 SSMs are: a PCA-based SSM, two RBF-KPCA based SSMs (gamma=0.1 and 1, where gamma is the parameter in RBF kernel function [46]), a PF-KPCA based SSM and an ICA based SSM.

The compactness is often used in statistical models to quantify the efficiency of the model in describing the total variance in the population [12]. The compactness ability can be measured as the cumulated variance, and is defined as:

$$\mathrm{C}(q) = \frac{\sum_{i=1}^{q} \lambda_i}{\sum_{i=1}^{p} \lambda_i} \tag{4}$$

where $q$ is the number of the components that are used in the model and $\lambda_i$ is the eigen value of the $i_{th}$ component [27]. $p$ denotes the number of all components of the SSM. Generally speaking, when the compactness curve quickly converges to one, it indicates that most of the variation in the dataset is captured with fewer components. A reduced number of components may simplify the system and significantly accelerate the computing speed when using the SSM to fit a new scan or predict a new shape. Figure 8 shows the compactness of the different generated SSMs as the function of the number of components. Though the compactness of all SSMs rises with the increase of the number of components, the compactness of the PCA-based SSM increases faster than other SSMs. To reach 80% of the shape variance, only two principal components are needed for the PCA-based SSM while for RBF-KPCA, forty-four components are needed regardless of the values of the gamma. For PF-KPCA and ICA, four and twenty-four components are respectively required to realize the same result. Using 20 components, the compactness is about 98% for PCA-based SSM, and 96% for PF-KPCA. However, ICA-based SSM can only achieve 74% of compactness with same number of components. For the two RBF-KPCA-based SSMs, the compactness only reaches approximately 36% with 20 components.

The generalization represents the ability of the SSM in describing the instance that is not in the training set. To measure the generalization ability, a leave-one-out strategy was adopted. Using this method, an SSM was built using all models but one in

the dataset, then the excluded model was fitted by the SSM where the weight of each component that yields the best fit to the model was found through minimizing the RMSE between two models. This process iterated and the mean of the minimized RMSEs was taken as the generalization $\mathrm{G}(q)$, where $q$ is the number of components used in the SSM. Fig. 9 presents $\mathrm{G}(q)$ of the five SSMs regarding different number of components used in the model. Increasing the number of components constantly decreases the generalization error for all models, and the PCA, PF-KPCA, and ICA models respectively achieved 1.29 ± 0.16 mm, 1.57 ± 0.47 mm, and 1.17 ± 0.17 mm accuracy when 15 PCs were used. The generalization error for RBF-KPCA-based model was higher relative to the other three models, which was found to be 2.39 ± 1.56 mm, and 2.09 ± 1.27 mm when gamma was set to 0.1 and 1, respectively. With 20 PCs, the accuracy further improved to 1.21 ± 0.14 mm, 1.44 ± 0.39 mm and 1.08 ± 0.15 mm for PCA, PF-KPCA and ICA. Even the results for RBF-KPCA-based models became better, they were 2.25 ± 1.5 mm (gamma=0.1) and 1.99 ± 1.25 mm (gamma=1). In summary, the performance of PCA-based and ICA-based SSMs were the best regarding generalization ability, where the ICA based SSM had slightly smaller error.

Specificity ($S_{spe}(q)$) describes the ability of the SSM can generate the new instance that are similar to the models in the training set. It is measured by 1) generating a population of randomly and uniformly distributed models based on the generated SSM; 2) measuring the average distance of the generated models to their nearest models in the training set. The specificity is defined as:

$$S_{spe}(q) = \frac{1}{N_{spe}} \sum_{u=1}^{N_{spe}} min\|M_u(q) - M'_u\|; (q = 1, \cdots, p) \quad (5)$$

where $M_u(q)$ is the sample that generated with the first $q$ components in the SSM, and $p$ is the number of all components in the SSM. $N_{spe}$ denotes the number of randomly generated models and was taken as 10000 in this paper. The closest sample in training set to $M_u(q)$ is denoted as $M'_u$. The specificity for PCA, PF-KPCA, RBF-KPCA and ICA is shown in Fig. 10, where the specificity of RBF-KPCAs (gamma= 0.1 and 1) are the smallest, and the result of PF-KPCA is larger than the other four models.

In summary, regarding the compactness of the SSMs, fewer components are needed when using PCA or PF-KPCA. However, the generalization error of the PF-KPCA-based SSM shows a larger error than the PCA-based SSM. By balancing the needed accuracy, the computational efficiency, the SSM built based on PCA with 20 PCs was selected as the hand SSM for its high compactness and relatively high accuracy.

**5. EXPERIMENT & DISCUSSION**

A self-developed Python program was used to analyze the data and build the model. The computing time of registering each scan to the template was less than one minute with an Intel i7-6700 processor at 4G HZ. For the data analysis, it took less than 5 minutes to compute each SSM (PCA, RBF-KPCA, PF-KPCA, ICA) using the same computer. The proposed SSM generated based on posture invariant hand models can approach a given 3D scan with relatively high accuracy. To verify this, we constructed another SSM directly from the acquired scans without posture correction. In Fig. 11, the first six components of the posture invariant SSM and the SSM without posture correction are

shown. Fig. 12 illustrates the difference between the compactness of the two SSMs regarding the number of principal components, where the posture invariant SSM is more compact than the SSM without posture correction. For example, in order to describe 90% of the shape variation, the SSM without posture correction needs eight components while for the posture invariant SSM, only four components are needed. When we inspect the SSM without posture correction, we can also notice that the posture variation is also considered as a shape variation.

An SSM with high compactness has many advantages. As discussed in previous sections, it will save computing time when the SSM is used to fit a scan and it will decrease the risk of overfitting. In general, the more principle components present in the shape model, the worse the precision of the estimated shape model parameters [14].

To validate the accuracy of the proposed SSM, we acquired a new 3D scan of human hand using the close-range photogrammetry hand scanner. The scan was aligned to the standard gesture first, then the above two SSMs were used to fit the scan. The fitting errors of the two SSMs are presented in Fig. 13(a) regarding the number of principal components. It can be found that the proposed posture invariant SSM outperformed the SSM without posture correction regardless of the number of PCs used in the model. Fig. 13(b) shows the fitting errors where twenty PCs were used regarding two models, respectively. It can be found that in this case, the RMSE was 4.91 mm by fitting the SSM without posture correction to the hand. The RMSE was lowered to 0.73 mm when it is fitted with the posture invariant SSM.

The fitted model in Fig. 13(b) has a standard posture. To further validate the usability of the proposed SSM, we restored the fitted SSM to the original posture of another scan using the embedded skeleton and the LBS algorithm. This process is presented in Fig. 14 step by step. First, the acquired 3D scan (in yellow) was aligned with the template and deformed to the standard posture (in red), then the SSM was used to fit the scan with the standard posture (in green). In this case, the RMSE between the SSM and the deformed scan was measured as 0.63 mm. The fitted model was restored to the original posture of the scan (in magenta) using the inverse of the deformation matrix identified in the first step. The RMSE between the restored SSM (in magenta) and the original 3D scan (in yellow) was 1.69 mm. This error was larger than the RMSE between two models in the standard posture, mainly due to the errors introduced by the LBS algorithm. Though the LBS algorithm was developed to simulate the free-form deformation in reality, there are gaps in-between. This highlights the need for an SSM with different postures constructed from 4D scanning data for a more accurate approximation of human hand in different postures.

High accuracy, posture invariant models, are essential to the adoption and wider usage of human digital models in applications such as human-integrated digital twin applications, virtual reality, anthropometric study, and personalized product design. Figure 15 presents a case study of a personalized design of 3D printed hand splint, which is used to stabilize and support the thumb. In this design application, the developed SSM was integrated into the computational design approach of the hand splint based on Rhino® Grasshopper®. In the figure, the mean model of the hand was used in the center

of the figure where at the left, the PC1 of the SSM was adjusted to +3σ, and at the right, the PC1 of the SSM was set as -3σ. By adjusting the parameters of each PC of the SSM, the model was able to quickly fit an individual human hand and the personalized hand splint can be regenerated automatically.

At this stage, the proposed 3D SSM only has one “valid” posture and other postures can be achieved by skeleton based deformation algorithms, e.g. linear blend skinning. Current research is directed toward a 4D SSM, where multiple “valid” postures will be established. It is expected by establishing those “key frames”, the deformation of human hand will be more accurate in the simulation of the movement of the human hands.

## 6. CONCLUSION

In this paper, we proposed a posture invariant hand SSM to overcome the posture variances among different 3D scans. Using an Möbius sphere-based algorithm, the correspondence between 3D scans of human hands can be established. By embedding an articulated skeleton in each scan, the postures of all scans were aligned to a standard posture. Using those scans and based on a comparison of the performance of several SSMs using the principal component analysis, the RBF-Kernel Principal Component Analysis, the PF-Kernel Principal Component Analysis and the Independent Component Analysis methods, we selected the PCA method to build the posture invariant SSM. The results of the leave-one-out experiments indicated that the proposed SSM is able to reach an accuracy of 1.21± 0.14 mm in fitting 3D hand scans. Further

comparison with an SSM without posture correction indicated that though it might be expensive in the construction, the proposed posture invariant SSM can approach a human hand with much higher accuracy and/or less PCs.

**ACKNOWLEDGMENT**

The authors of this paper would like to express their appreciation to Ms. Tessa T. W. Essers, Mr. Bertus J. Naagen, Mr. Adrie Kooijman, Mr. Martin Verwaal for the fruitful discussions and kind assistance during the experiment.

**FUNDING**

The work of Yusheng Yang is sponsored by the program of China Scholarships Council (No. 201806890056). This project is partially funded by the Dutch NWO Next UPPS (Ultra-Personalized Products and Services) project.

**NOMENCLATURE**

| | |
|---|---|
| $V$ | The set of vertices in the mesh |
| $F$ | The set of faces in the mesh |
| $N_v$ | The number of vertices |
| $N_f$ | The number of triangles |
| $v_j$ | The 3D Cartesian coordinate of the $j_{th}$ vertex in $V$ |
| $f_k$ | The $k_{th}$ triangle in $F$ |
| $N$ | The number of scans |
| $D_M$ | The dataset of all scans |
| $M_i$ | The $i_{th}$ model in $D_M$ |
| $K_{M_i}$ | The signals for the hand scan $M_i$ |
| $K_{M_T}$ | The signals for the template $M_T$ |
| $R^*$ | The rotation |
| $M_T$ | The template model |
| $B$ | The bone of the hand skeleton |
| $J$ | The joint of the hand skeleton |
| $N_b$ | The number of bones |
| $L$ | The hand skeleton |
| $Q_B$ | The rotation matrix of bone $B$ |
| $l_B$ | The length of bone $B$ |
| $T_B$ | The transformation matrix of bone $B$ |
| $G(M)$ | The posture of the model $M$ |
| $H_B$ | The transformation matrix from the world coordinate to the local coordinate of bone $B$ |
| $T_{p_B}$ | The parent coordinate system corresponding to $T_B$ |
| $\mathbb{T}_i$ | The relative rotation matrix of bone $B_i$ |
| $w_i(v_j)$ | The weight function of the $i_{th}$ bone associated with the vertex $v_j$ |
| $D_M^c$ | The dataset that all postures of scans are aligned |
| $m$ | The index of the vertex |
| $V_m^{mean}$ | The mean position of $m_{th}$ vertex |
| $V_{M_{new}}$ | The vertexes of the new generated model based on SSM |
| $V_{M_{mean}}$ | The mean model for SSM |
| $N_p$ | The number of feature vectors that used for reconstruction |
| $\gamma_j$ | The contribution of the component $PC_j$ |
| $PC_j$ | The $j_{th}$ principal component |
| $\emptyset(\cdot)$ | The reconstruction |
| $\mathrm{C}(q)$ | The compactness of SSM with $q$ components |
| $\mathrm{G}(q)$ | The generalization ability of the SSM with $q$ components |
| $S_{spe}(q)$ | The specificity of the SSM with $q$ components |
| $M_u(q)$ | The sample that generated with the first $q$ components in SSM |
| $N_{spe}$ | The number of randomly generated models |
| $M_u'$ | The closest sample in training set to $M_u(q)$ |

**REFERENCES**


[1] M. Grieves, “Digital twin: manufacturing excellence through virtual factory replication,” *White Pap.*, vol. 1, pp. 1–7, 2014.

[2] D. Jones, C. Snider, A. Nassehi, J. Yon, and B. Hicks, “Characterising the Digital Twin: A systematic literature review,” *CIRP J. Manuf. Sci. Technol.*, vol. 29, pp. 36–52, 2020.

[3] C. Emmanouilidis *et al.*, “Enabling the human in the loop: Linked data and knowledge in industrial cyber-physical systems,” *Annu. Rev. Control*, vol. 47, pp. 249–265, 2019.

[4] D. Romero, J. Stahre, and M. Taisch, “The Operator 4.0: Towards socially sustainable factories of the future,” *Comput. Ind. Eng.*, vol. 139, no. November 2019, 2020.

[5] B. R. Barricelli, E. Casiraghi, J. Gliozzo, A. Petrini, and S. Valtolina, “Human Digital Twin for Fitness Management,” *IEEE Access*, vol. 8, pp. 26637–26664, 2020.

[6] C. H. Chu, I. J. Wang, J. B. Wang, and Y. P. Luh, “3D parametric human face modeling for personalized product design: Eyeglasses frame design case,” *Adv. Eng. Informatics*, vol. 32, pp. 202–223, 2017.

[7] R. Wang, C.-F. Chen, H. Peng, X. Liu, O. Liu, and X. Li, “Digital Twin: Acquiring High-Fidelity 3D Avatar from a Single Image,” 2019.

[8] Y. Hasson *et al.*, “Learning joint reconstruction of hands and manipulated objects,” in *Proceedings of the IEEE Conference on Computer Vision and Pattern Recognition*, 2019, pp. 11807–11816.

[9] A. Yu, K. L. Yick, S. P. Ng, and J. Yip, “Case study on the effects of fit and material of sports gloves on hand performance,” *Appl. Ergon.*, vol. 75, no. March 2018, pp. 17–26, 2019.

[10] S.-Y. Baek and K. Lee, “Statistical foot-shape analysis for mass-customisation of footwear,” *Int. J. Comput. Aided Eng. Technol.*, vol. 8, no. 1–2, pp. 80–98, 2016.

[11] G. Harih and B. Dolšak, “Tool-handle design based on a digital human hand model,” *Int. J. Ind. Ergon.*, vol. 43, no. 4, pp. 288–295, 2013.

[12] J. Van Houtte *et al.*, “An Articulating Statistical Shape Model of the Human Hand,” in *International Conference on Applied Human Factors and Ergonomics*, 2018, pp. 433–445.

[13] R. J. Schwarz and C. L. Taylor, “The anatomy and mechanics of the human hand,” *Artif. Limbs*, vol. 2, no. 2, pp. 22–35, 1955.

[14] F. Danckaers, T. Huysmans, A. Hallemans, G. De Bruyne, S. Truijen, and J. Sijbers, “Posture normalisation of 3D body scans,” *Ergonomics*, vol. 62, no. 6, pp. 834–848, 2019.

[15] J. A. Martin, J. Ramsay, C. Hughes, D. M. Peters, and M. G. Edwards, “Age and grip strength predict hand dexterity in adults,” *PLoS One*, vol. 10, no. 2, 2015.

[16] H. Endo and K. Kawahara, “Gender differences in hand stability of normal young people assessed at low force levels,” *Ergonomics*, vol. 54, no. 3, pp. 273–281, 2011.

[17] B. Schölkopf, A. Smola, and K.-R. Müller, “Kernel principal component analysis,” in

*International conference on artificial neural networks*, 1997, pp. 583–588.

[18] M. Üzümcü, A. F. Frangi, J. H. C. Reiber, and B. P. F. Lelieveldt, "Independent component analysis in statistical shape models," in *Medical Imaging 2003: Image Processing*, 2003, vol. 5032, pp. 375–383.

[19] A. Hyvärinen and E. Oja, "Independent component analysis: algorithms and applications," *Neural networks*, vol. 13, no. 4–5, pp. 411–430, 2000.

[20] S.-Y. Baek and K. Lee, "Parametric human body shape modeling framework for human-centered product design," *Comput. Des.*, vol. 44, no. 1, pp. 56–67, 2012.

[21] K. M. Robinette, H. Daanen, and E. Paquet, "The CAESAR project: a 3-D surface anthropometry survey," in *Second International Conference on 3-D Digital Imaging and Modeling (Cat. No. PR00062)*, 1999, pp. 380–386.

[22] B. Allen, B. Curless, and Z. Popović, "The space of human body shapes: reconstruction and parameterization from range scans," *ACM Trans. Graph.*, vol. 22, no. 3, pp. 587–594, 2003.

[23] H. Seo and N. Magnenat-Thalmann, "An automatic modeling of human bodies from sizing parameters," in *Proceedings of the 2003 symposium on Interactive 3D graphics*, 2003, pp. 19–26.

[24] O. Sorkine and M. Alexa, "As-rigid-as-possible surface modeling," *EurographicS Symp. Geom. Process.*, pp. 548–557, 2007.

[25] N. Hasler, C. Stoll, M. Sunkel, B. Rosenhahn, and H. Seidel, "A statistical model of human pose and body shape," in *Computer graphics forum*, 2009, vol. 28, no. 2, pp. 337–346.

[26] M. Loper, N. Mahmood, J. Romero, G. Pons-Moll, and M. J. Black, "SMPL: A Skinned Multi-Person Linear Model," *ACM Trans. Graph.*, vol. 34, no. 6, p. 248, 2015.

[27] S. Wuhrer, C. Shu, and P. Xi, "Posture-invariant statistical shape analysis using Laplace operator," *Comput. Graph.*, vol. 36, no. 5, pp. 410–416, 2012.

[28] F. Danckaers, T. Huysmans, A. Hallemans, G. De Bruyne, S. Truijen, and J. Sijbers, "Full body statistical shape modeling with posture normalization," in *International Conference on Applied Human Factors and Ergonomics*, 2017, pp. 437–448.

[29] I. Oikonomidis, N. Kyriazis, and A. A. Argyros, "Full DOF tracking of a hand interacting with an object by modeling occlusions and physical constraints," in *Proceedings of the IEEE International Conference on Computer Vision*, 2011, pp. 2088–2095.

[30] S. Sridhar, F. Mueller, A. Oulasvirta, and C. Theobalt, "Fast and robust hand tracking using detection-guided optimization," in *Proceedings of the IEEE Conference on Computer Vision and Pattern Recognition*, 2015, pp. 3213–3221.

[31] S. Sridhar, A. Oulasvirta, and C. Theobalt, "Interactive markerless articulated hand motion tracking using RGB and depth data," *Proc. IEEE Int. Conf. Comput. Vis.*, pp. 2456–2463, 2013.

[32] A. Tkach and A. Tagliasacchi, "Sphere-Meshes for Real-Time Hand Modeling and Tracking," vol. 35, no. 6, 2016.

[33] J. Romero, D. Tzionas, and M. J. Black, "Embodied Hands: Modeling and Capturing Hands and Bodies Together," *ACM Trans. Graph*, vol. 36, no. 4, p. 17, 2017.

[34] O. A. van Nierop, A. van der Helm, K. J. Overbeeke, and T. J. P. Djajadiningrat, “A natural human hand model,” *Vis. Comput.*, vol. 24, no. 1, pp. 31–44, 2008.
[35] K. Li and X. Qian, “Direct diffeomorphic reparameterization for correspondence optimization in statistical shape modeling,” *Comput. Des.*, vol. 64, pp. 33–54, 2015.
[36] B. Amberg, S. Romdhani, and T. Vetter, “Optimal step nonrigid ICP algorithms for surface registration,” in *2007 IEEE Conference on Computer Vision and Pattern Recognition*, 2007, pp. 1–8.
[37] Q. Chen and V. Koltun, “Robust nonrigid registration by convex optimization,” in *Proceedings of the IEEE International Conference on Computer Vision*, 2015, pp. 2039–2047.
[38] J. Ma, J. Zhao, and A. L. Yuille, “Non-rigid point set registration by preserving global and local structures,” *IEEE Trans. image Process.*, vol. 25, no. 1, pp. 53–64, 2015.
[39] S. C. Lee and M. Kazhdan, “Dense Point-to-Point Correspondences Between Genus-Zero Shapes,” in *Computer Graphics Forum*, 2019, vol. 38, no. 5, pp. 27–37.
[40] A. Neophytou and A. Hilton, “Shape and pose space deformation for subject specific animation,” in *2013 International Conference on 3D Vision-3DV 2013*, 2013, pp. 334–341.
[41] B.-K. Park, J. C. Lumeng, C. N. Lumeng, S. M. Ebert, and M. P. Reed, “Child body shape measurement using depth cameras and a statistical body shape model,” *Ergonomics*, vol. 58, no. 2, pp. 301–309, 2015.
[42] A. Jain, T. Thormählen, H.-P. Seidel, and C. Theobalt, “MovieReshape: Tracking and Reshaping of Humans in Videos,” *ACM Trans. Graph.*, vol. 29, no. 6, p. 1, 2010.
[43] L. Pishchulin, S. Wuhrer, T. Helten, C. Theobalt, and B. Schiele, “Building statistical shape spaces for 3D human modeling,” *Pattern Recognit.*, vol. 67, pp. 276–286, 2017.
[44] B. Allen, B. Curless, and Z. Popović, “The space of human body shapes: Reconstruction and parameterization from range scans,” *ACM SIGGRAPH 2003 Pap. SIGGRAPH ’03*, pp. 587–594, 2003.
[45] M. Kirschner, M. Becker, and S. Wesarg, “3D active shape model segmentation with nonlinear shape priors,” in *International Conference on Medical Image Computing and Computer-Assisted Intervention*, 2011, pp. 492–499.
[46] S. Faghih Roohi and R. Aghaeizadeh Zoroofi, “4D statistical shape modeling of the left ventricle in cardiac MR images,” *Int. J. Comput. Assist. Radiol. Surg.*, vol. 8, no. 3, pp. 335–351, May 2013.
[47] H.-T. Lübbers, L. Medinger, A. Kruse, K. W. Grätz, and F. Matthews, “Precision and Accuracy of the 3dMD Photogrammetric System in Craniomaxillofacial Application,” *J. Craniofac. Surg.*, vol. 21, no. 3, pp. 763–767, May 2010.
[48] Y. Yang, W. S. Elkhuizen, T. Hou, T. T. W. Essers, and Y. Song, “Optimal Camera Configuration for 3D Scanning of Human Hand,” in *International Design Engineering Technical Conferences and Computers and Information in Engineering Conference*, 2019, vol. 59179, p. V001T02A047.

[49] Z. Ben Azouz, M. Rioux, C. Shu, and R. Lepage, “Characterizing human shape variation using 3D anthropometric data,” *Vis. Comput.*, vol. 22, no. 5, pp. 302–314, 2006.

[50] R. Dyke, C. Stride, Y. Lai, and P. Rosin, “SHREC-19: Shape correspondence with isometric and non-isometric deformations,” 2019.

[51] M. Kazhdan, J. Solomon, and M. Ben-Chen, “Can mean-curvature flow be modified to be non-singular?,” in *Computer Graphics Forum*, 2012, vol. 31, no. 5, pp. 1745–1754.

[52] J. Sun, M. Ovsjanikov, and L. Guibas, “A concise and provably informative multi-scale signature based on heat diffusion,” in *Computer graphics forum*, 2009, vol. 28, no. 5, pp. 1383–1392.

[53] S. Khamis, J. Taylor, J. Shotton, C. Keskin, S. Izadi, and A. Fitzgibbon, “Learning an efficient model of hand shape variation from depth images,” *Proc. IEEE Comput. Soc. Conf. Comput. Vis. Pattern Recognit.*, vol. 07-12-June, pp. 2540–2548, 2015.

[54] D. J. Tan *et al.*, “Fits like a glove: Rapid and reliable hand shape personalization,” *Proc. IEEE Comput. Soc. Conf. Comput. Vis. Pattern Recognit.*, vol. 2016-Decem, pp. 5610–5619, 2016.

[55] N. Magnenat-Thalmann, R. Laperrire, and D. Thalmann, “Joint-dependent local deformations for hand animation and object grasping,” in *In Proceedings on Graphics interface’88*, 1988.

[56] A. Jacobson, I. Baran, J. Popovic, and O. Sorkine, “Bounded biharmonic weights for real-time deformation.,” *ACM Trans. Graph.*, vol. 30, no. 4, p. 78, 2011.

[57] J. C. Gower, “Generalized procrustes analysis,” *Psychometrika*, vol. 40, no. 1, pp. 33–51, 1975.

[58] B. Schölkopf, S. Mika, A. Smola, G. Rätsch, and K.-R. Müller, “Kernel PCA pattern reconstruction via approximate pre-images,” in *International Conference on Artificial Neural Networks*, 1998, pp. 147–152.

[59] Q. Wang, “Kernel principal component analysis and its applications in face recognition and active shape models,” *arXiv Prepr. arXiv1207.3538*, 2012.

[60] M. A. Styner *et al.*, “Evaluation of 3D correspondence methods for model building.,” *Inf. Process. Med. Imaging*, vol. 18, pp. 63–75, 2003.

**LIST OF FIGURES**



**LIST OF TABLES**

**Table 1. List of hand models in the literature**

| Sources | Hand model | Geometry | DOF | Accuracy(mm) | Accuracy measures | Statistical Model |
|---|---|---|---|---|---|---|
| Oikonomidis et al. [29] | 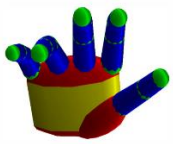 | Cones, Spheres, ellipsoid | 26 (including 6 for global transformation) | **HOPE**[a]: 3-29<br>**PEHI**[b]: 12-47 | **MAE**[c] of landmarks | NO |
| Remero et al. [33] |  | Vertexes and faces | 15 (without global transformation) | 0.93 | **MAE**[c] between surfaces | YES |
| Sridhar et al. [31] | 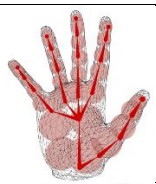 | Vertices and faces | 26 (including 6 for global transformation) | 13.24 | **MAE**[c] of landmarks over all frames | NO |
| Tkach et al. [32] | 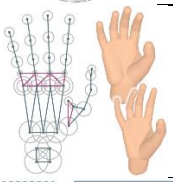 | Sphere - mesh | 26 (including 6 for global transformation) | N/A | N/A | NO |
| Khamis et al. [53] | 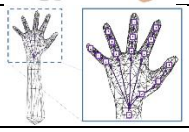 | Vertices and faces | 28 (including 6 for global transformation) | **RMSE**[d]: 2.8-3.2<br>**MAE**[c]: 1.8-2.1 | **RMSE**[d] and **MAE**[c] between surfaces | NO |

a: Hand-object pose estimation
b: Pose estimation of hands in isolation
c: Mean absolute error
d: Root mean square error
Pictures courtesy of the corresponding articles

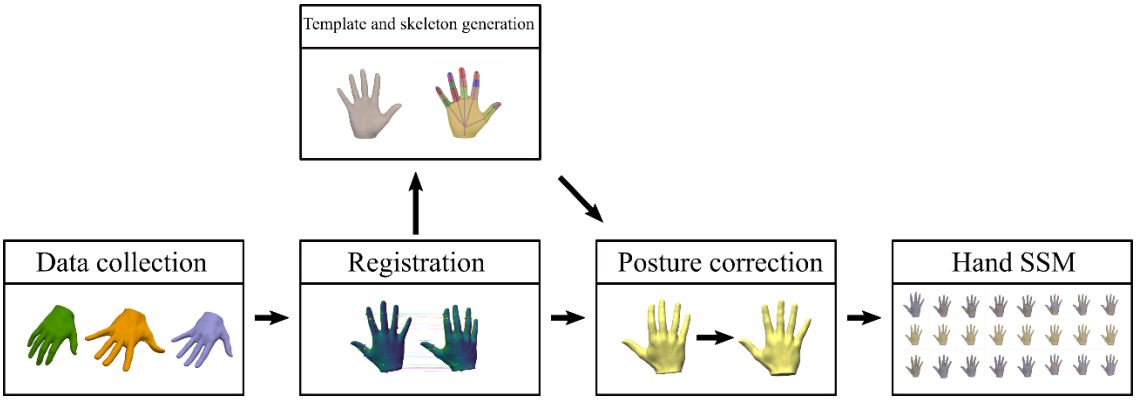


Fig. 1 The proposed approach for building a posture invariant hand SSM.

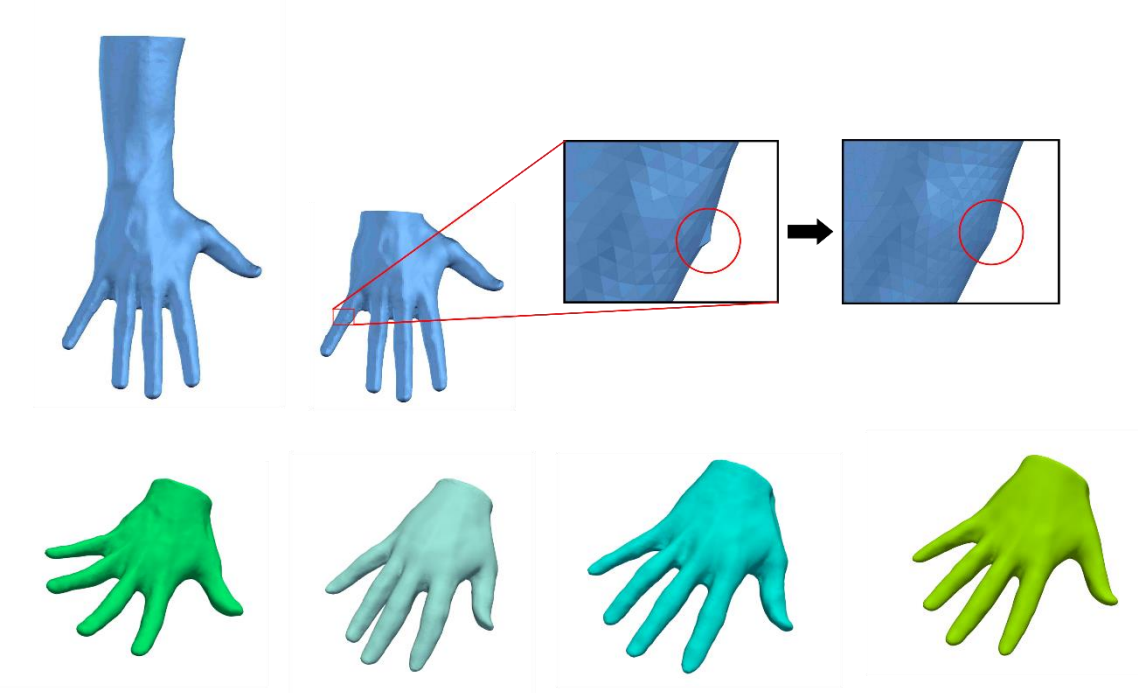

Fig. 2 3D scans of human hands (Top row: The raw data of a 3D scan and an example of post-processing, where a spike was removed. The bottom row: 4 examples of 3D scans after post-processing.).

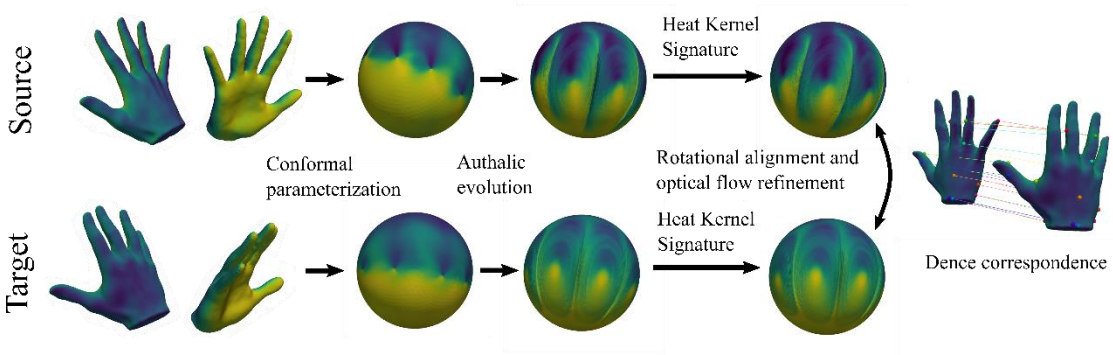


Fig. 3 Establishing correspondence between the template and a scan with different postures.

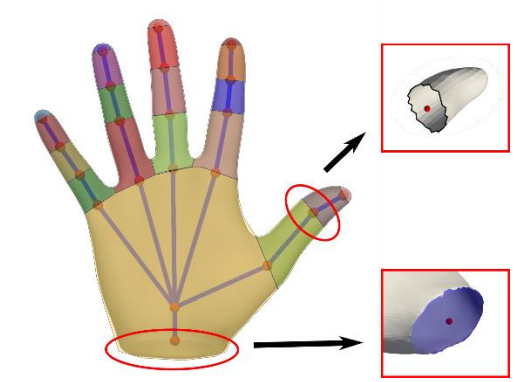

(a) Segmented hand model and the embedded skeleton

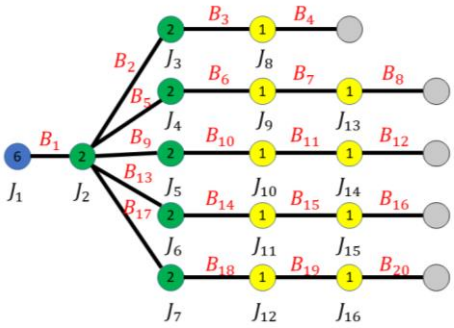


(b) The hierarchical relationship of bone segments and joints in the skeleton. The number in a circle means the number of DOFs that this joint has, circles in gray are the fingertips, which have no DOF.

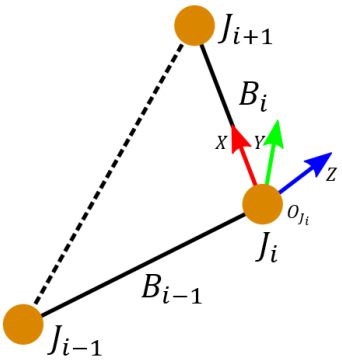


(c) The local coordinate of $B_i$.

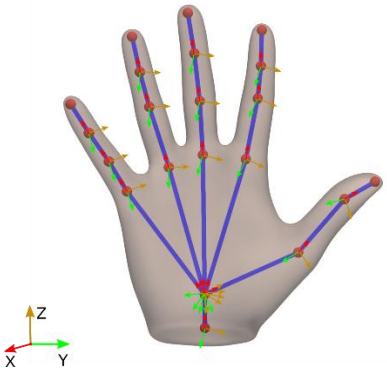


(d) Coordinates of all joints.

Fig. 4 Embedding a skeleton in the hand.

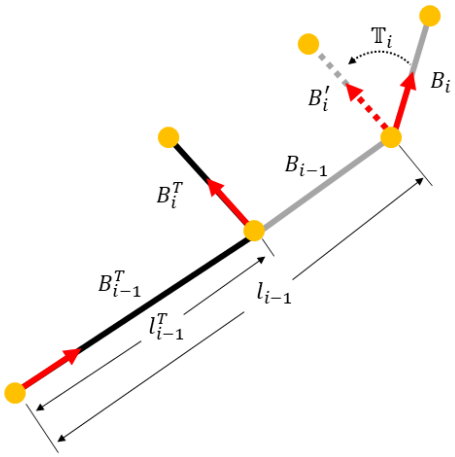


Fig. 5 Align $B_i$ to $B_i^T$ for posture correction.

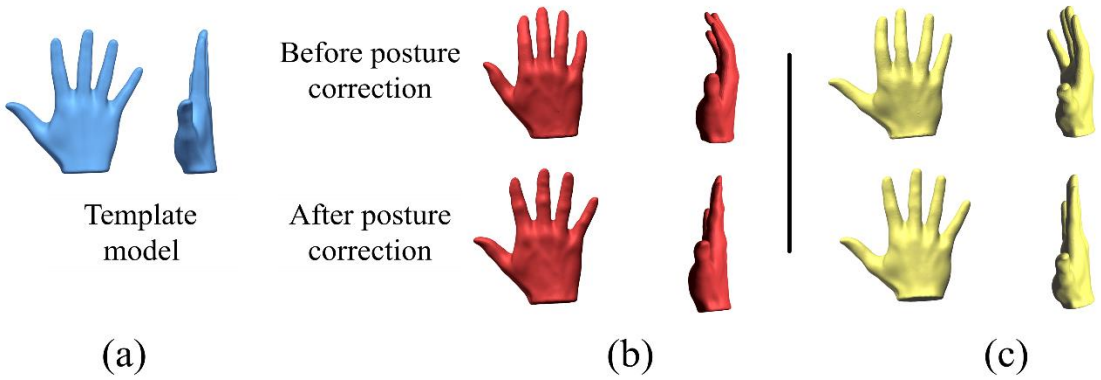


Fig. 6 Posture correction. a) The template hand model. b, c) Two examples of the posture correction. In each example, the first row shows the dorsal and side views of the original model before posture correction. The second row presents the result after posture correction.

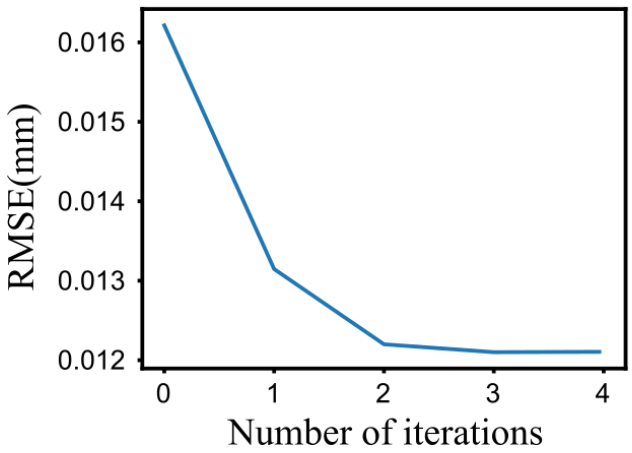


Fig. 7 The RMSE between $M_{mean}$ and $M_{new}$ regarding the number of iterations in Algorithm 1.

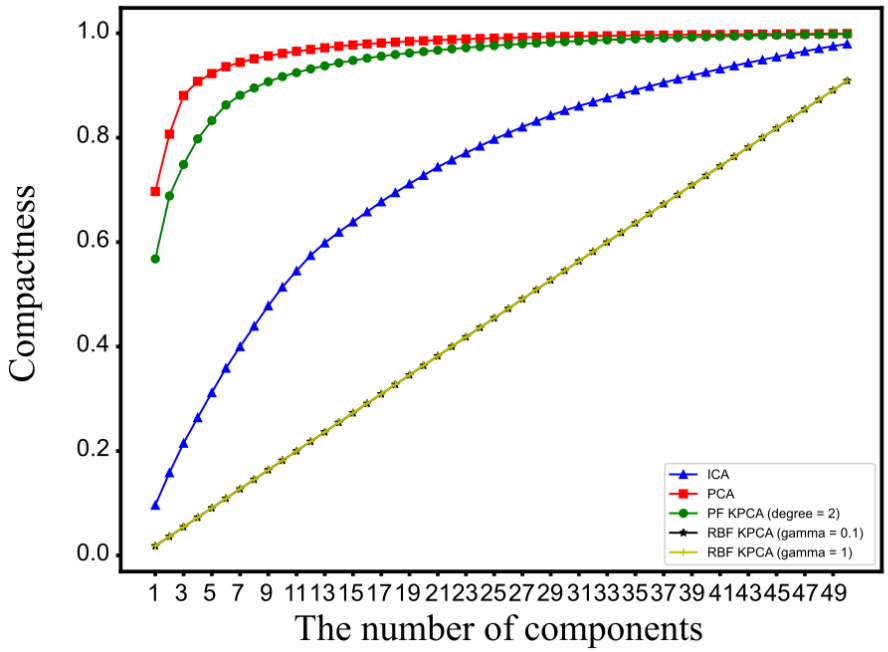


Fig. 8 The compactness regarding the number of PCs.

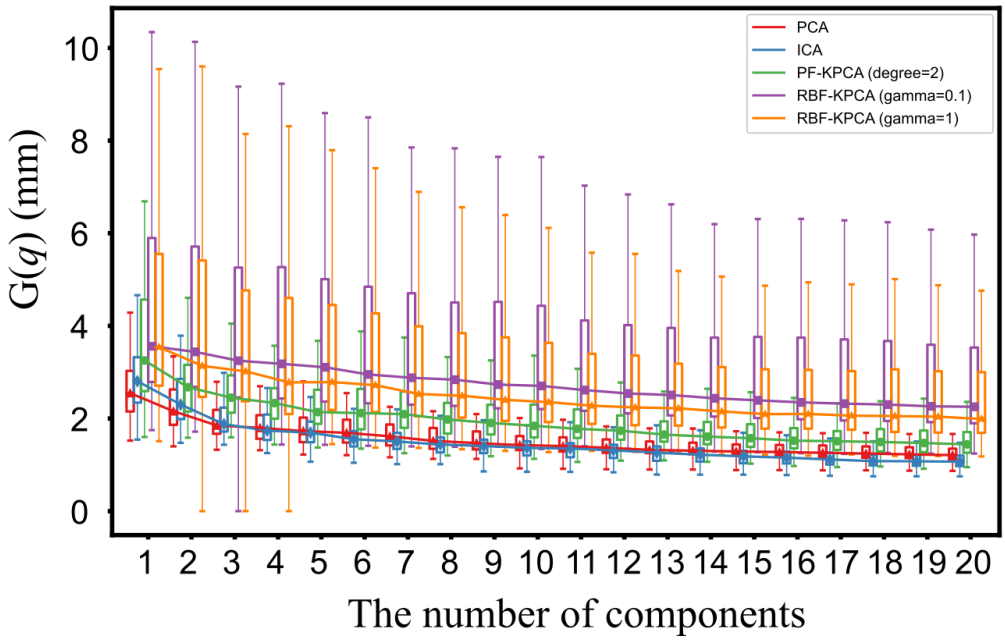


Fig. 9 The fitting error regarding the number of components.

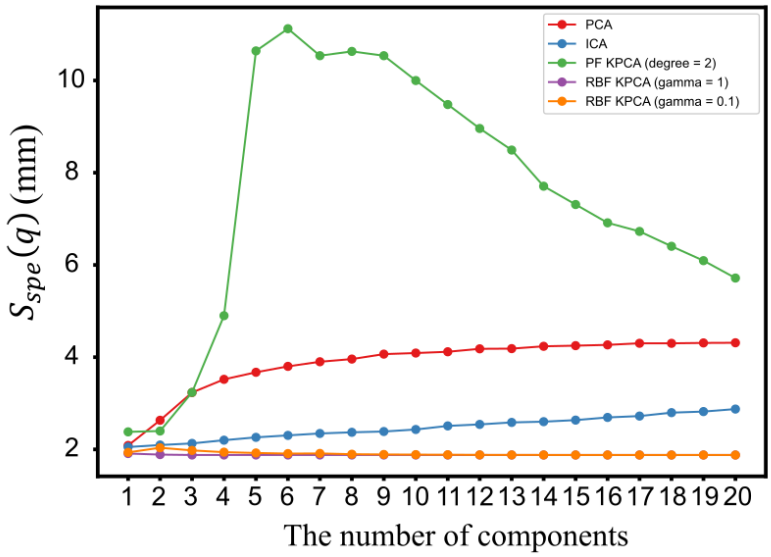


Fig. 10 The specificity regarding the number of components.

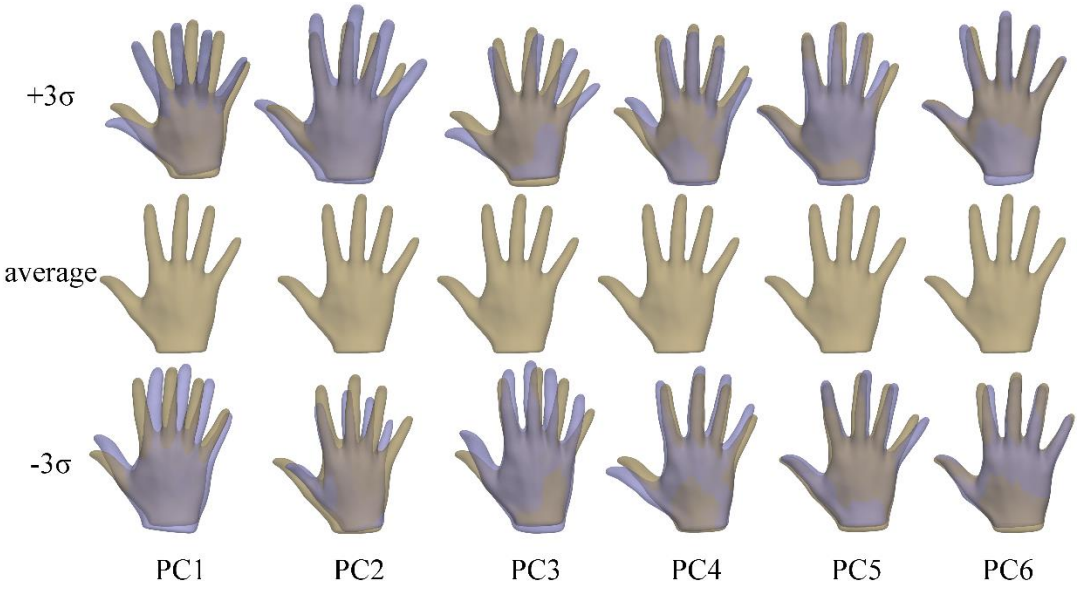


(a) Effects of the first six components (from -3σ to +3σ) of the SSM without posture correction. Deviations among the fingers are clearly visible

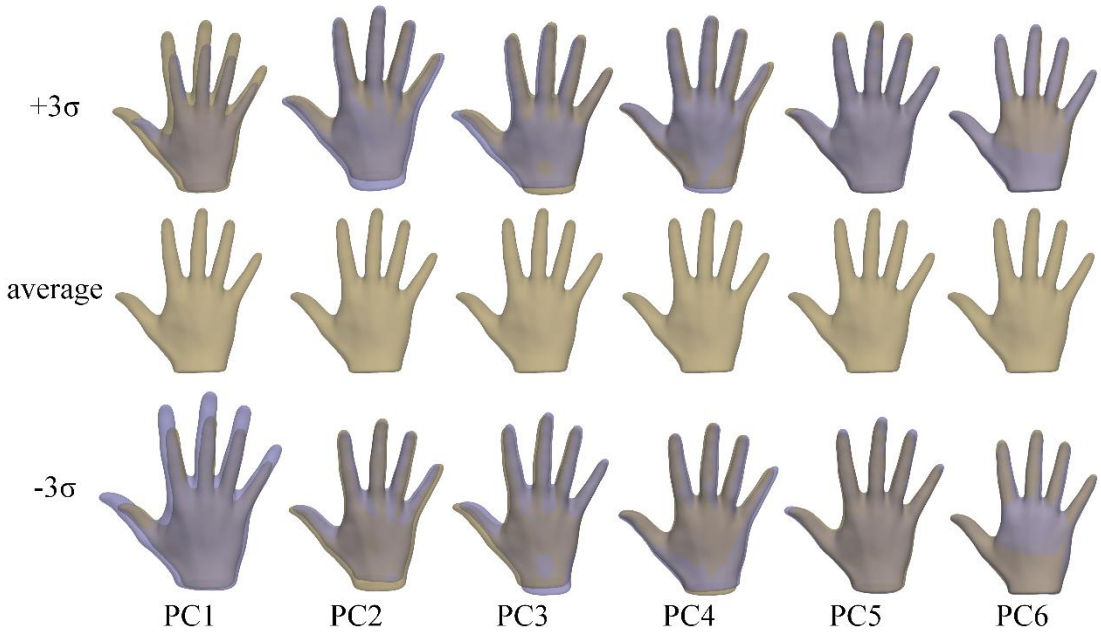


(b) Effects of the first six components (from -3σ to +3σ) of the posture invariant SSM. Less deviations are observed regarding the posture

Fig. 11 Effects of the first six components of the SSM without posture correction and the posture invariant SSM.

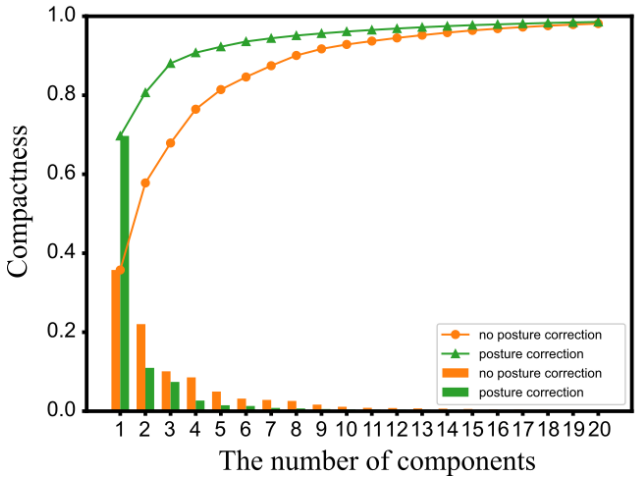


Fig. 12 Comparison of the compactness for the posture invariant SSM and the SSM without posture correction. The bar graph shows the compactness of each PC, and the line graph illustrates the cumulative compactness of two SSM models.

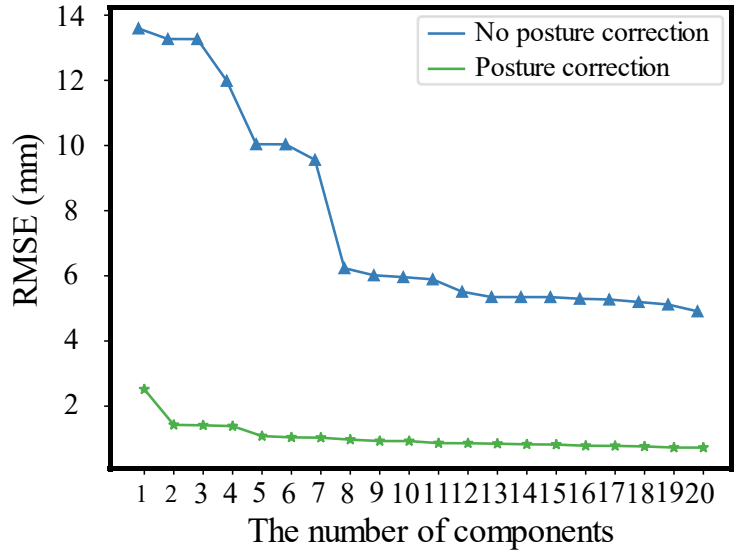


(a)

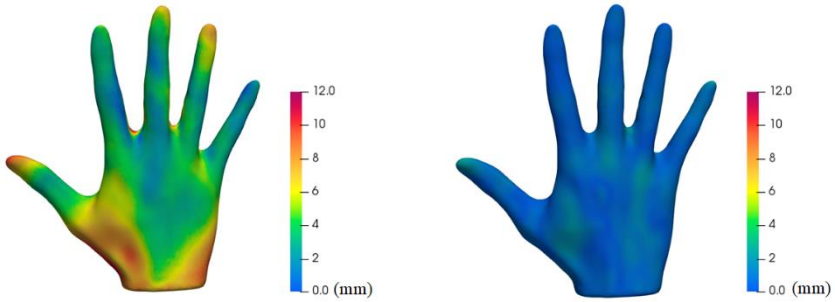


Fitting the scan with the SSM without posture correction

Fitting the scan with the posture correction SSM

(b)

Fig. 13 The fitting error comparation between two SSMs. (a) The model fitting error regarding the number of components. (b) The error distribution of fitting the scan with two SSMs (20 PCs).

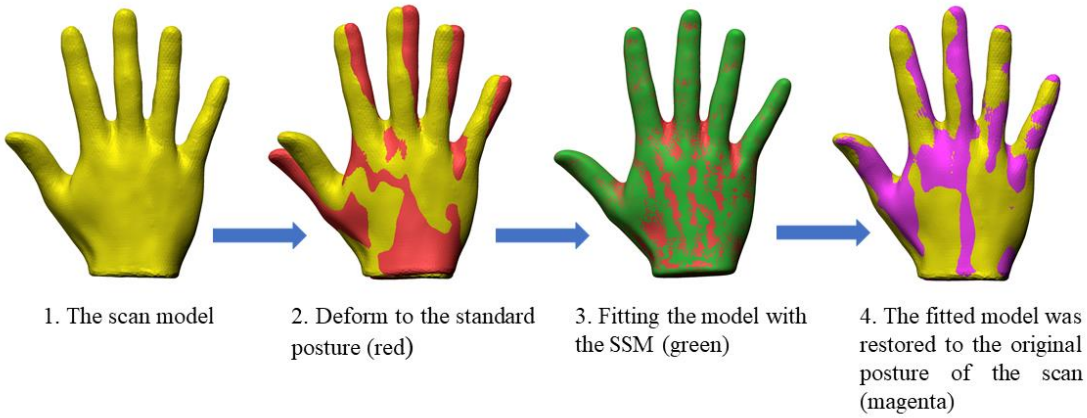


Fig. 14 Restoring the original posture of the fitted model.

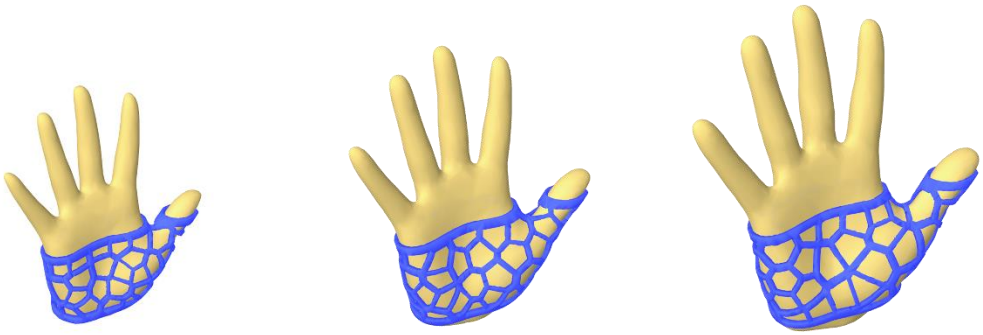

Fig. 15 Personalized hand split design based on the proposed hand SSM